# Electrical Control of the Magnetic State of Fe

Lukas Gerhard[1], Toyo Kazu Yamada[1,2], Timofey Balashov[1], Albert F. Takács[3], Rien J. H. Wesselink[1,4], Markus Däne[5,6], Michael Fechner[5], Sergey Ostanin[5], Arthur Ernst[5], Ingrid Mertig[5,7], and Wulf Wulfhekel[1]

[1]Physikalisches Institut, Karlsruhe Institute of Technology (KIT), 76131 Karlsruhe, Germany
[2]Graduate School of Advanced Integration Science, Chiba University, Chiba 263-8522, Japan
[3]Faculty of Physics, Babes-Bolyai University, 400084 Cluj-Napoca, Romania
[4]Faculty of Science and Technology and MESA+ Institute for Nanotechnology,University of Twente, 7500 AE Enschede,The Netherlands
[5]Max-Planck-Institut für Mikrostrukturphysik, 06120 Halle, Germany
[6]Materials Science and Technology Division, Oak Ridge National Laboratory, Oak Ridge, TN 37831 USA
[7]Martin-Luther-Universität Halle-Wittenberg, Institut für Physik, 06099 Halle, Germany

**Magneto-electric coupling offers a new pathway to information storage in magnetic memory devices. This phenomenon has been observed in various materials ranging from insulators to semiconductors. In bulk metallic systems, magneto-electric coupling has been disregarded as the electric field cannot enter bulk metals. In this work, we show that a substantial magneto-electric coupling exists in metallic Fe nano-islands grown on Cu(111). Using the electric field in the tunnel junction of a scanning tunneling microscope, the magnetic order parameter and the crystal structure of Fe was changed on the nanometer scale. This allows high density nonvolatile information storage by means of magneto-electric coupling in a simple metallic system.**

***Index Terms*—Hard disks, magnetoelectric effects, magnetic memory, scanning probe microscopy.**

## I. Introduction

THE possibility to change the magnetic state of a nanostructure in a controlled way by means other than a magnetic field attracted significant interest in the last years. Magneto-electric coupling (MEC) links the magnetic state to the electric field. The ultimate dream is to use MEC in magnetic data storage devices to write magnetic bits. Since the discovery of the first multiferroic materials almost thirty years ago [1], only little attention has been payed to MEC in metals. Most materials showing MEC are multiferroic insulators, where ferroelectric and ferromagnetic order parameters coexist [2]–[4]. In these materials, the electric polarization can be changed by applying an external electric field [5]–[7]. The change of the electric polarization is caused by a displacement of the positive and negative ions with respect to each other. This displacement in turn may influence the magnetic state. The microscopic processes that lead to MEC are rather complex and still lacking a complete theoretical understanding. As in metals any external electric field is screened by the formation of a surface charge, MEC cannot be found in a bulk metallic system. This surface screening charge, however, is not only formed by the motion of the mobile electrons, but also by a slight displacement of the positively charged atomic cores in the top atomic layer [8]. Supposed in a metallic system the magnetic configuration changes upon lattice deformations on the picometer scale, the possibility of MEC in metallic nanostructures would be opened. In this combined theoretical and experimental work, we show that MEC is present in magnetic nano-structures and magnetic information can be written, stored, and read on the nanometer scale.

Manuscript received January 03, 2011; accepted January 11, 2011. Date of current version May 25, 2011. Corresponding author: W. Wulfhekel (e-mail: wulf.wulfhekel@kit.edu).

Digital Object Identifier 10.1109/TMAG.2011.2107506

## II. The Model System Fe/Cu(111)

Fe is a suitable material for MEC as it exhibits remarkable phase properties: the magnetic order of Fe delicately depends on the unit cell volume [9]. Here, self-organized Fe nano-structures were used as a model system for MEC in metals. At room temperature, a sub-monolayer (ML) amount of Fe was deposited on atomically clean Cu(111) by molecular beam epitaxy in ultra high vacuum (UHV) leading to the formation of 2 ML high Fe islands [10]. MEC of these samples was then studied with a scanning tunneling microscopy (STM) operating at 4.5 K in UHV. For this particular system of Fe on Cu(111), Biedermann and colleagues showed that two different phases coexist [11]. The center of the islands exactly follows the face-centered cubic (fcc) stacking of the Cu(111) substrate while the rim adopts a body-centered cubic (bcc) like structure similar to the ground state of bulk Fe. Our STM measurements revealed the same atomic configuration. Especially a perfectly hexagonal structure was observed in the center and a bcc-like stacking at the borders that is accompanied by a misalignment of the atomic lines by small angels with respect to the fcc lattice [11], [12]. As the bcc structure appears higher than the fcc structure by about 30 pm, the two phases can easily be distinguished in STM images (see inset in Fig. 1). The magnetic order of the two phases is not directly accessible experimentally. Performing spin-polarized STM experiments we excluded magnetic structures that are laterally inhomogeneous. In order to distinguish the remaining two laterally homogeneous magnetic orders (ferromagnetic and layer-wise antiferromagnetic), we performed spatially resolved scanning tunneling spectroscopy (STS) measurements on the island center and rim. In an extended Tersoff-Hamann model, the differential conductance measured by STS can be identified with the local density of states (LDOS) [13]. Best agreement is found when normalizing the measured $dI/dU$ signal over the tunneling matrix element $T$ [14]. The resulting experimental spectra are shown in Fig. 1 (solid lines) [12]. These spectra

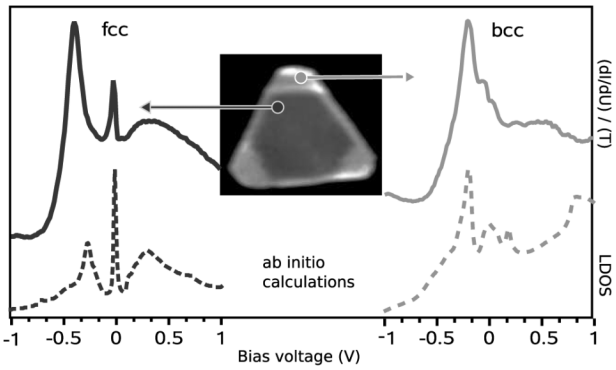


Fig. 1. Scanning tunneling spectra (solid lines) at positions indicated in the inset in comparison with *ab-initio* calculations of the LDOS (dashed lines). Spectra taken on the fcc phase (left side) only match with the calculated LDOS of an antiferromagnetic structure, while spectra taken on the bcc phase (right side) only match with the LDOS of a ferromagnetic bcc structure.

were compared to theoretical calculations of the LDOS. We performed the first principles calculations of the LDOS assuming different magnetic configurations of a fcc and a bcc bilayer Fe double-layer on a semi-infinite Cu(111) substrate. The experimental spectrum of the fcc center of the Fe islands matches only with a theoretical LDOS of a layer-wise antiferromagnetic fcc structure and an interlayer distance of 2.00 Å (see Fig. 1, left side, dashed line). The rims of the island show experimental spectra that exclusively fit the LDOS of a ferromagnetic Fe bilayer and an interlayer distance of 2.12 Å (see Fig. 1, right side, dashed line). All other combinations did not fit (not shown, see [12]). This identifies the darker phase in the STM images of the Fe islands as an antiferromagnetic fcc structure and the brighter phase as a ferromagnetic bcc structure.

## III. Simulation of MEC

As theoretical calculations and STM measurements show a small height difference between the antiferromagnetic fcc and the ferromagnetic bcc phase, the possibility to change the interatomic distance between first and second Fe layer by applying an electric field would allow to influence the magnetic structure via MEC. We therefore performed first principles calculations using the Vienna ab initio simulation package (VASP) within the density functional theory approach [12]. In a first step only vertical relaxations of a bilayer Fe slab on a Cu(111) substrate were considered in a plate capacitor simulating an electric field of 1 GV/m. In accordance to the simple model presented in the introduction, the simulations show the formation of a surface charge by the displacement of the electrons and the atomic cores in the top Fe layer as can be seen in Fig. 2, [12]. In the vicinity of the positive electrode the atomic cores are repelled thereby reducing the Fe interlayer distance [see Fig. 2(a)]. A negative electrode attracts the atomic cores thereby increasing the interlayer distance [see Fig. 2(b)]. Additionally, the calculations of the total energy show an antiferromagnetic alignment of the two Fe layers for reduced interlayer distance in a positive electric field and a ferromagnetic alignment in the case of an increased interlayer distance in a negative electric field. As the atomically resolved STM measurements for Fe islands on Cu(111) revealed a coexistence of fcc and bcc structures [11], also lateral displacements of the topmost Fe atoms were considered being responsible for the transitions from fcc to bcc. This diffusionless transition is called martensitic, which consists basically of an in-plane displacement of the top Fe atoms from the fcc threefold hollow sides to the bcc twofold bridge positions [11]. Therefore, in a

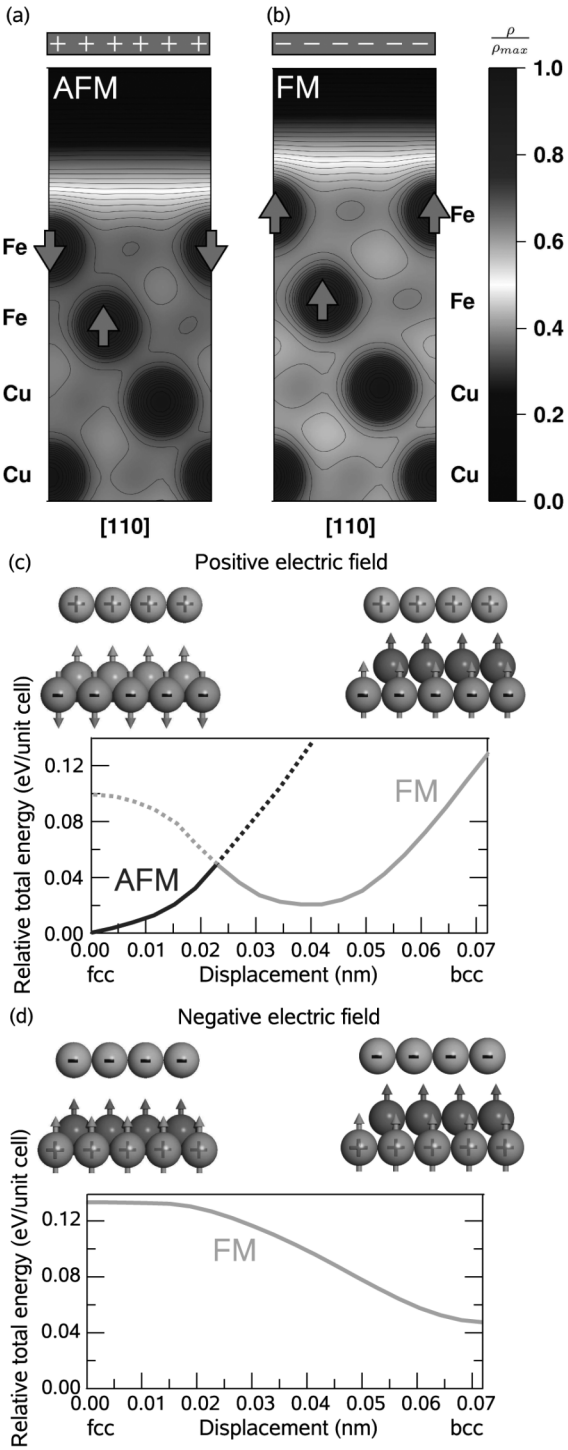


Fig. 2. Simulation of electric field-induced structural changes of a bilayer Fe slab on a Cu(111) substrate [12]. (a), (b) Charge density of 2 Fe layers and 2 Cu layers of the substrate shows a reduced interlayer distance for a positive electric field (a) and an increased interlayer distance for negative electric field (b). The structural changes lead to an antiferromagnetic alignment for the reduced (a) and to a ferromagnetic alignment for the enhanced interlayer distance (b). (c), (d) Total energy per unit cell as function of a lateral displacement of the top layer Fe atoms along the martensitic transition from fcc to bcc (from left to right). The energetically most favorable configurations are antiferromagnetic fcc for a positive electric field (c) and ferromagnetic bcc for a negative electric field (d).

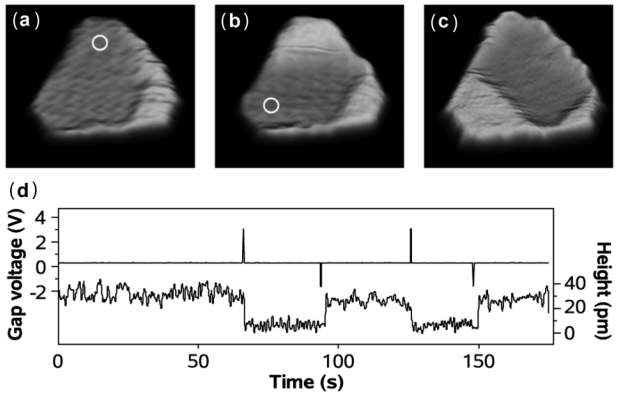


Fig. 3. STM images of the same Fe island before (a) and after (b), (c) applying negative electric field pulses at indicated positions. (d) Applied gap voltage and height underneath the STM tip as function of time demonstrating the reproducibility of the switching.

second step, the total energy was calculated for the top layer Fe atoms in an electric field, vertically relaxed at each lateral position following the path from the fcc to the bcc position [12]. Both ferromagnetic and antiferromagnetic configurations were considered, each in positive and negative electric fields. This results in an energy landscape shown in Fig. 2(c), (d). In a positive electric field the antiferromagnetic fcc configuration is lowest in energy per unit cell and is well separated by a barrier of about 20 meV from the bcc configuration that is unstable [see Fig. 2(c)]. In an applied electric field of negative polarity, the fcc configuration is unstable and the ferromagnetic bcc configuration is favored [see Fig. 2(c)]. This implies a coupling of the magnetic order to the electric field and a stability of the two phases with respect to a transition to the other one.

## IV. Experimental Observation of MEC With STM

As the theoretical calculations predict a MEC in the Fe islands, the influence of an electric field in the tunneling gap of an STM was also experimentally studied. Thus, voltage pulses with the tip positioned above the island were given to induce a local and large electric field. In this way, STM can be used at low bias voltages to image the state of the island and at high bias voltages to manipulate the magnetic state. In this sense an STM is a unique tool to investigate MEC, as it offers the opportunity to control huge electric fields on the nanometer scale in combination with its ability of imaging with atomic resolution. Fig. 3(a) shows an STM image of an Fe island recorded at low electric field. We applied an electric field pulse of $-1$ GV/m lasting 50 ms. Afterwards another STM image of this islands is recorded at low electric field, shown in Fig. 3(b). It can be clearly seen that in full accordance to the theoretical predictions the area underneath the tip was switched from the ferromagnetic bcc to the antiferromagnetic fcc state. The original state is regained by applying an electric field of negative polarity. This switching is a reproducible process as can be seen in Fig. 3(d). The apparent height of the structure underneath the tip at a fixed position can be switched back and forth. When applying positive electric fields an antiferromagnetic fcc structure was induced, when applying negative electric fields a ferromagnetic bcc structure was obtained. Measuring STS spectra before and after the switching, we confirmed that not only the crystallographic structure changes, but also the magnetic state is switched in accordance. Thus, it is indeed possible to write single magnetic bits on the nanometer scale by electric fields. As the bcc Fe structure exhibits a smaller in-plane lattice constant than that of the Cu(111) substrate, the bcc structure only occurs at the edges of the triangular islands where the in-plane stress is lower. An increase of the bcc area leads to an increase of the in-plane stress in the island and thus favors the fcc configuration. There are two consequences for the switching. First, a bistability of antiferromagnetic fcc and ferromagnetic bcc can only be found close to the island edge. Second, the overall stress in the Fe island is limited. As can be seen in the two consecutive images Fig. 3(b) and (c), switching two edges, the third edge switches from ferromagnetic bcc to antiferromagnetic fcc.

## V. Verification of MEC as Switching Mechanism

In the *ab-initio* calculations, the tunneling junction was modeled by a plate capacitor in order to understand the influence of the electric field. In the STM measurements; however, a tunneling current is present as well. The influence of the tunneling current has to be considered to exclude other mechanisms than MEC. We therefore investigated the relation between the two basic parameters of the STM setup, the applied bias voltage and the tunneling current. At a fixed lateral position of the tip, a tunneling current was chosen and the applied bias voltage is ramped while recording the height of the sample underneath the tip. The inset in Fig. 4(a) shows that at a certain critical voltage the structure suddenly changes from the lower fcc to the higher bcc. The voltage ramp is repeated at a series of different tunneling currents, resulting in different critical voltages. The pairs of critical voltages and corresponding tunneling currents are plotted in Fig. 4(a). This graph shows the phase diagram of the Fe bilayer islands as function of the measured critical voltage and the tunneling current. This relation between voltage and current can be used to compare the switching process in the experiment with different possible models for the phase transition.

Under the assumption, that the transition is caused by the energy of the tunneling electrons, for example by inducing an inelastic excitation the a phase transition only depends on the applied bias voltage. As can be seen in Fig. 4(a) ($U = const.$), this model does not fit this data. Another possibility is a mechanism depending on the tunneling current, e.g., due to the spin torque [15], spin accumulation [16], or electro-migration. The corresponding straight line in Fig. 4(a) ($I = const.$) fails in reproducing the experimental results. A third possibility for a phase transition might relate to local heating by the tunneling current. In this model the dissipated power would be the critical value, but as can be seen in Fig. 4(a) ($P = U * I = const.$), this can also be excluded. Finally we consider the overlap of the wave functions of tip and sample, i.e., a mechanical contact or partial chemical bond formation. This is directly linked to the distance between tip and sample. In order to relate the distance between tip and sample with the applied bias voltgage and the tunneling current, we use a simple well known approximation for the tunneling current in an STM setup: $I \propto U \cdot e^{((-2\sqrt{2m\Phi})/\hbar)d}$, where $\Phi$ is the apparent barrier height [17] and $d$ is the distance between tip and sample. This model also clearly deviates from the experimental findings as can be seen in Fig. 4(a) ($d = const.$).

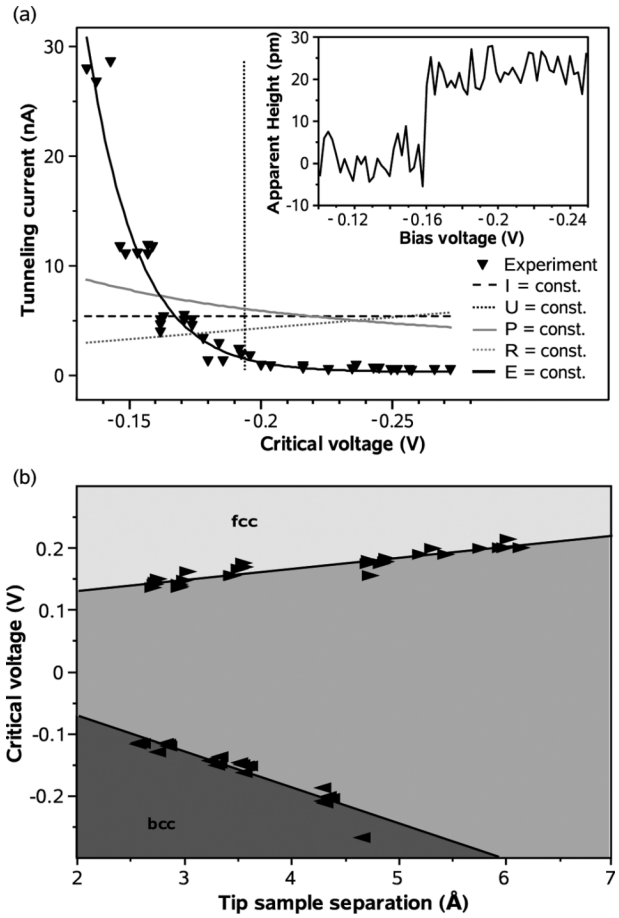


Fig. 4. Systematic study of the switching mechanism via MEC. (a) Relation between the critical voltage and the tunneling current [12]. For each tunneling current, the bias voltage was ramped up, until the critical voltage is reached and the phase transition from fcc to bcc is observed (see inset). This results in pairs of tunneling current and critical voltage corresponding to the phase boundary (black triangles) and offers the possibility to exclude other mechanisms than MEC. (b) Phase diagram with the critical voltage plotted against the tip sample distance.

We are left with the switching to be driven by MEC. To evaluate the scenario of a constant electric field $E = U_c/d$, we used the approximation for the tunneling current as function of the bias voltage mentioned above. This model fits the experimental data well [black line in Fig. 4(a)] and hence explains the phase transition. At a closer look, we find two parameters that have to be determined in this relation: the resistance in contact, for $d = 0$, and the apparent barrier height $\Phi$. The latter can be determined experimentally by approaching the STM tip to the surface in a controlled way. Thus, the increase of $I$ is measured as function of $d$. From the observed rise of $I$ the effective barrier height $\Phi$ is determined. Additionally, we assume a resistance of $R_0 = 12.9\ \mathrm{k}\Omega$ for the metallic point contact at zero distance. With this, we can estimate $d$ from the bias voltage and tunneling current and re-plot the critical bias voltage $u_c$ against $d$ [Fig. 4(b)]. As expected, the voltage can be fitted as a linear function of the distance. Thus the slope gives the value of the critical electric field, that is determined to values between 3 and $9 \times 10^8\ \mathrm{V/m}$, similar to those used in the calculations. In order to provide a full phase diagram we extended this voltage distance relation to positive electric fields. As can be seen in Fig. 4(b), also the switching from bcc to fcc is driven by an electric field, only the absolute value necessary to induce the transition is slightly lower. In the range of intermediate electric fields, we find a hysteretic behavior. This finally provides a complete set of experiments, proving that MEC in Fe nano-islands can be used to reproducibly write and read nonvolatile magnetic bits with electric fields.

In summary, we have shown that magnetic information can be written, stored and read only by electric fields. While the results demonstrate large MEC at metallic surfaces, for applications, the vacuum barrier should be replaced by an oxide layer to allow integration into solid state memories.

## ACKNOWLEDGMENT

T. K. Yamada acknowledges funding by the Alexander-von-Humbold foundation, A. Ernst and W. Wulfhekel by the Deutsche Forschungsgemeinschaft (projects ER 340/4-1, WU 349/8-1), A. F. Takács for the Sectoral Operational Program for Human Resources Development 2007-2013 and the European Social Fund (POSDRU 89/1.5/S/60189).

## REFERENCES

[1] G. A. Smolenskii and I. E. Chupis, "Ferroelectromagnetism," *Soviet Physics Uspekhi* vol. 25, no. 7, p. 475, 1982.
[2] T. Lottermoser, T. Lonkai, U. Amann, D. Hohlwein, J. Ihringer, and M. Fiebig, "Magnetic phase control by an electric field," *Nature* vol. 430, pp. 541–544, 2004.
[3] T. Kimura, T. Goto, H. Shintani, K. Ishizaka, T. Arima, and Y. Tokura, "Magnetic control of ferroelectric polarization," *Nature* vol. 426, pp. 55–58, 2003.
[4] N. A. Spaldin and M. Fiebig, "The renaissance of magnetoelectric multiferroics," *Science* vol. 309, no. 5733, pp. 391–392, 2005.
[5] C. Ederer and N. A. Spaldin, "Magnetoelectrics: A new route to magnetic ferroelectrics," *Nat. Mater*, vol. 3, no. 12, pp. 849–851, Dec. 2004.
[6] C. Ederer and N. A. Spaldin, "Origin of ferroelectricity in the multiferroic barium fluorides $bamf_4$: A first principles study," *Phys. Rev. B*, vol. 74, no. 2, p. 024102, Jul. 2006.
[7] Y.-H. Chu, L. W. Martin, M. B. Holcomb, M. Gajek, S.-J. Han, Q. He, N. Balke, C.-H. Yang, D. Lee, W. Hu, Q. Zhan, P.-L. Yang, A. Fraile-Rodriguez, A. Scholl, S. X. Wang, and R. Ramesh, "Electric-field control of local ferromagnetism using a magnetoelectric multiferroic," *Nat. Mater*, vol. 7, no. 6, pp. 478–482, Jun. 2008.
[8] J. Weissmüller, R. N. Viswanath, D. Kramer, P. Zimmer, R. Wüurschum, and H. Gleiter, "Charge-induced reversible strain in a metal," *Science*, vol. 300, pp. 312–315, 2003.
[9] V. L. Moruzzi, P. M. Marcus, K. Schwarz, and P. Mohn, "Ferromagnetic phases of bcc and fcc Fe, Co, and Ni," *Phys. Rev. B*, vol. 34, pp. 1784–1791, 1986.
[10] J. Shen, P. Ohresser, C. V. Mohan, M. Klaua, J. Barthel, and J. Kirschner, "Magnetic moment of fcc Fe(111) ultrathin films by ultrafast deposition on Cu(111)," *Phys. Rev. Lett.*, vol. 80, no. 9, pp. 1980–1983, Mar. 1998.
[11] A. Biedermann, W. Rupp, M. Schmid, and P. Varga, "Coexistence of fcc- and bcc-like crystal structures in ultrathin Fe films grown on Cu(111)," *Phys. Rev. B* vol. 73, no. 16, p. 165418, 2006.
[12] L. Gerhard, T. K. Yamada, T. Balashov, A. F. Takács, R. J. H. Wesselink, M. Däne, M. Fechner, S. Ostanin, A. Ernst, I. Mertig, and W. Wulfhekel, "Magnetoelectric coupling at metal surfaces," *Nat. Nano.*, vol. 5, no. 11, pp. 792–797, Nov. 2010.
[13] J. Tersoff and D. R. Hamann, "Theory and application for the scanning tunneling microscope," *Phys. Rev. Lett.*, vol. 50, no. 25, pp. 1998–2001, Jun. 1983.
[14] V. A. Ukraintsev, "Data evaluation technique for electron-tunneling spectroscopy," *Phys. Rev. B*, vol. 53, no. 16, pp. 11176–11185, Apr. 1996.
[15] J. C. Slonczewski, "Conductance and exchange coupling of two ferromagnets separated by a tunneling barrier," *Phys. Rev. B*, vol. 39, no. 10, p. 6995, 1989.
[16] F. J. Jedema, A. T. Filip, and B. J. van Wees, "Electrical spin injection and accumulation at room temperature in an all-metal mesoscopic spin valve," *Nature*, vol. 410, no. 10, p. 345, 2001.
[17] J. G. Simmons, "Generalized formula for the electric tunnel effect between similar electrodes separated by a thin insulating film," *J. Appl. Phys.*, vol. 34, no. 6, p. 1793, 1963.